Materials Advances

ROYAL SOCIETY OF CHEMISTRY

PAPER

View Article Online
View Journal | View Issue

Cite this: *Mater. Adv.*, 2022, 3, 4252

Development and structural analysis of dual-thermo-responsive self-assembled zwitterionic micelles†

Dandan Zhao,[a] Robin Rajan,[a] Shin-ichi Yusa,[b] Masaru Nakada[c] and Kazuaki Matsumura*[a]

Received 16th December 2021,
Accepted 6th April 2022

DOI: 10.1039/d1ma01189h

rsc.li/materials-advances

Multi-stimuli-responsive materials may dominate next-generation drug delivery systems. Herein, dual-thermo-responsive micelles were prepared by introducing cholesterol chloroformate to facilitate the spontaneous self-assembly of graft polymers prepared by combining two charged polymers, poly-sulfobetaine and carboxylated ε-poly-L-lysine. This polymerization was controlled by reversible addition fragmentation chain transfer polymerization. Turbidimetry measurements and temperature-dependent ^{1}H NMR spectroscopy were used to investigate the phase transition behaviors; transmission electron microscopy and atomic force microscopy were used to determine the morphology of the micelles. The dependence of self-assembled structures on temperature was investigated through ultra-small-angle X-ray scattering (USAXS). The micelles formed spherical shapes in water which was confirmed by TEM and AFM. Interestingly, different, temperature-dependent micelle size change behaviors were observed through dynamic light scattering, Ultraviolet-visible (UV-Vis) spectroscopy, and USAXS; this might be due to the concentration-dependent hierarchical phase transition. This study provides crucial information on the mesoscopic structure of the micelles, and will enable greater control over their transition temperatures for numerous biomaterial applications.

Introduction

Micelles that can be employed as a water-insoluble drug delivery system and simultaneously enhance disease diagnostics have attracted considerable attention.[1–3] Amphiphilic polymers can form micelles in aqueous solutions by self-assembly; the hydrophobic core of the micelles can load water-insoluble drugs,[4,5] thereby enhancing the solubility of hydrophobic drugs, and the presence of a hydrophilic shell can increase the stability of the micelles in an aqueous environment and prolong the metabolism time.[6,7] Most antitumor drugs, such as paclitaxel, camptothecin, and cabazitaxel are water-insoluble, which limits their applicability; this issue can be solved by the use of micelles to deliver such drugs.[8–10] Additionally, employing micelles may also suppress the side effects of the drugs and increase the efficacy of the active pharmaceutical ingredient. Although some micelle formulations, such as Genexol PM, have been applied in clinical treatment,[11] several challenges hinder the widespread use of micelles, with the main limitation being the absence of disease specificity.[12]

To overcome these limitations, stimuli-responsive micelle systems that can change their physical or chemical properties with changes in the environment, such as pH, light, and temperature, are being investigated extensively.[13–15] In particular, multi-stimuli systems are interesting, owing to the presence of additional properties that are capable of switching states under two different conditions, and have been employed in various applications,[16–19] including delivering more than two drugs using a single system.[20–22] Among them, temperature-responsive micelle systems have been preferred.[23] The temperature of tumor tissues is reported to be slightly higher than that of the normal tissues, owing to faster metabolism.[24–28] Moreover, tissues can withstand temperatures of up to 43 °C for long periods of time, without any irreversible consequences.[29] Therefore, micelles of temperature-responsive polymers may have the ability of targeted release at the delivery site.[30]

Poly(*N*-isopropylacrylamide) (PNIPAAM) is one of the most studied thermo-responsive polymers, and in an aqueous solution, this polymer undergoes a coil–globule transition with an increase in temperature.[31] Moreover, its transition temperature is around 32 °C, which is close to the human physiological

[a] *School of Materials Science, Japan Advanced Institute of Science and Technology, 1-1 Asahidai, Nomi, Ishikawa, 923-1292, Japan. E-mail: mkazuaki@jaist.ac.jp*
[b] *Department of Applied Chemistry, Graduate School of Engineering, University of Hyogo, 2167 Shosha, Himeji, Hyogo, 671-2280, Japan*
[c] *Toray Research Center, Inc., 3-7 Sonoyama 3-chome, Otsu, Shiga, 520-8567, Japan*

† Electronic supplementary information (ESI) available. See DOI: https://doi.org/10.1039/d1ma01189h

temperature.[32–36] Our group previously reported polyampholytes exhibiting a novel lower critical solution temperature (LCST) property, and these were synthesized by modifying the free amino groups in ε-poly-L-lysine (PLL) with succinic anhydride (PLLSA) for cryopreservation applications.[37,38] The LCST of these polymers was found to depend significantly on their hydrophobicity, degree of substitution of the anhydride, and concentration of the polymer solution. Interestingly, unlike other LCST-type polymers, the LCST in PLLSA is accompanied by liquid–liquid phase separation and coacervate formation in the aqueous phase, differing from the conventional coil–globule transition.[39]

In contrast, polymers that tend to be insoluble at low temperatures and soluble at high temperatures are said to exhibit upper critical solution temperature (UCST) properties. Polymers such as poly(*N*-acryloyl glycinamide),[40,41] poly(acrylamide-*co*-acrylonitrile) (P(AAm-*co*-AN))[42] and poly(sulfobetaine) (PSPB)[43] have been found to exhibit UCST behavior. Among the UCST-type polymers, PSPB polymers have attracted the most attention.[44] Their protein-like structures provide high biocompatibility, and they exhibit several biomedical properties such as anti-biofouling,[45,46] cryopreservation,[47] and protein aggregation inhibition.[48–52]

A few thermo-responsive micelles have been reported, such as poly(ethylene glycol)-*co*-poly(acrylamide-*co*-acrylonitrile) (PEG-*co*-P(AAm-*co*-AN)),[42] poly(sulfobetaine methacrylate)-*block*-poly(*N*,*N*-dimethylaminoethyl methacrylate) (poly(SBMA)-*b*-poly(DMEMA)),[53] and poly(2-(*N*-morpholino)ethyl methacrylate)-*b*-poly(2-(diethylamino)ethyl methacrylate.[54] Notably, despite the great potential of these micelles for use in biomedical applications, their corresponding studies did not transition into *in vivo* or clinical studies, thereby suggesting the need for further development of these types of systems. Moreover, insufficient data are available on the microstructures of these micelles. Compared with PNIPAM, more factors affect the LCST of PLLSA and these parameters may provide information on a more complex mesoscopic structure of the systems that contain PLLSA blocks in the micelles. Therefore, detailed structural information studies are necessary not only for the PLLSA homopolymer, but also for complex polymer systems containing PLLSA.

Micellization has often been triggered by the introduction of cholesterol,[20] which is a highly hydrophobic polycyclic molecule, an essential component of mammalian cells, and is responsible for membrane fluidity and permeability, intracellular transport, signal transduction, and cell trafficking.[55–57] As cholesterol is associated with many membrane-related bioprocesses, the incorporation of cholesterol not only promotes polymer self-assembly in aqueous media but also enables easier crossing of the cellular membrane by micelles,[58,59] while enhancing the encapsulation of polycyclic drugs.[60] Meanwhile, the degradability of cholesterol also suppresses the damage caused by the micelles.

In our previous work, we successfully synthesized graft polymers by combining PLLSA and PSPB (PLLSA-*g*-PSPB).[61] These polymers exhibit UCST-LCST type dual-thermo-responsive property, and we found that they exhibited a suppression of protein aggregation and loaded proteins electrostatically and subsequently released them upon changing the pH. However, their linear structure did not exhibit a strong bonding between the polymer chain and the therapeutic agent, such as drugs or proteins, because electrostatic interactions are not sufficiently strong and cannot be used under all conditions. Therefore, in the present study, we optimized PLLSA-*g*-PSPB linear systems by modifying them with cholesterol to obtain micellar structures formed by self-assembly in an aqueous solution. These micelles exhibited dual-thermo-responsive properties owing to the presence of two different thermo-responsive polyampholyte blocks and hence can be a strong candidate in the field of thermo-responsive drug delivery systems. Structural analysis and soft matter characterization have been widely studied using synchrotron radiation X-rays because of their light which is brighter than conventional laboratory X-ray sources.[62] Ultra-small angle X-ray scattering (USAXS) has particularly been used to elucidate the structural information of the micelles in detail, and it revealed interesting contrasting phase separation behaviors between the two charged segments in the micelle. To the best of our knowledge, this is the first study to show the formation of dual thermo-responsive micelles made by the combination of two different polyampholytes.

Experimental

Materials

A 25% (w/w) PLL (molecular weight 4000) aqueous solution was purchased from JNC Corp. (Tokyo, Japan). The sulfobetaine monomer was donated by Osaka Organic Chemical Ind., Ltd. (Osaka, Japan) and used without further purification. Succinic anhydride (SA), 1-ethyl-3-(3-dimethylaminopropyl) carbodiimide hydrochloride, and *N*-hydroxysuccinimide (NHS) were purchased from Wako Pure Chemical Industries Ltd. (Osaka, Japan). 2-(Dodecylthiocarbonothioylthio)-2-methylpropionic acid (reversible addition fragmentation chain transfer (RAFT) agent), 4,4′-azobis-(4-cyanovaleric acid) (V-501, initiator), pyrene, and cholesterol were purchased from Sigma-Aldrich (St. Louis, MO) and used as received.

Carboxylated poly-L-lysine (PLLSA) and macro-chain transfer agent (macro-CTA; PLLSA-RAFT agent) were prepared according to a previously reported synthetic method.[61]

Synthesis of cholesterol chloroformate-modified Macro-CTA (PLLSA-cho-RAFT agent)

0.33 mmol PLLSA50 or PLLSA65 (numbers represent the degree of succinylation of amino groups of PLL by SA) was dissolved in 10 mL DMSO at 130 °C. After complete dissolution, 1 mL dichloromethane (DCM) containing 0.03 mmol cholesterol chloroformate (cho) solution was added to the DMSO solution. After 6 h, the solution was transferred to a dialysis membrane (MWCO 3.5 KDa, Repligen Corp. Waltham, MA, US) and dialyzed against water for 3 days. After dialysis, the polymer was washed with DCM, and the aqueous phase was dried in an oven, followed by vacuum drying to obtain the desired polymer.

RAFT Polymerization of PLLSA-cho-PSPB

SPB monomer (6.6 mmol) and V-501 (6.6 μmol) were dissolved in water (45 mL). In another vial, macro-cho-CTA (PLLSA50-cho-RAFT and PLLSA65-cho-RAFT agents, respectively) (33 μmol) were dissolved in DMSO. Then, the DMSO solution was added to the water solution, and the mixture was purged with nitrogen gas for 1 h and subsequently polymerized at 90 °C for 24 h. The ratio of [SPB monomer] : [V-501] : [macro-cho-CTA] was 1000 : 1 : 5. The polymer was then purified by dialysis against water for 3 days using a dialysis membrane (MWCO 14 kDa). After dialysis, the polymer was obtained by lyophilization.

Polymer characterization

All NMR spectra were recorded on a Bruker AV400 Avance III spectrometer operating at 400 MHz. The temperature-dependent ^{1}H NMR experiment of M1 in D_2O was performed in the temperature range of 15–75 °C in 10 °C intervals. The NMR data were analyzed using Topspin 3.5 software. The number of repeating units of the graft copolymers was estimated by ^{1}H NMR spectroscopy, and the number of free NH_2 groups was determined by a 2,4,6-trinitrobenzene sulfonic acid (TNBS) assay.[63]

Determination of critical micelles concentration (CMC)

The CMC of the self-assembled micelles was estimated using pyrene as a fluorescent probe. Four microliters of pyrene (1.0 mM in acetone) were transferred to a 10 mL test tube, followed by complete drying under a stream of nitrogen gas. Micelle solutions of varying concentrations were added to each tube (4 mL). Then, the solutions were sonicated for 30 min, followed by incubation at 60 °C for 3 h. After 3 h, the samples were allowed to cool overnight. The fluorescence of the solubilized pyrene was measured using a JASCO FP-8500 spectrofluorometer at room temperature from 350 to 450 nm with an excitation wavelength of 339 nm. The ratio of the intensities of the peaks at 394 and 373 nm was plotted against the concentration of micelles to obtain the CMC.

Particle size and zeta potential

The diameter and zeta potential of the micelles were determined using a Zetasizer 300 system (Malvern Instruments, Worcestershire, UK) equipped with a He–Ne laser with a wavelength of 633 nm and a scattering angle of 173°. Sample solutions were prepared at 0.1% (w/w) in distilled water.

Atomic force Microscopy (AFM)

AFM images were obtained using an AFM5000II SPA-400 (HITACHI) with a Si probe (SI-DF20, Seiko). The sample solution (0.1% w/w) was dropped onto a freshly cleaved mica surface and air-dried overnight prior to measurement at room temperature in the dynamic force microscope (DFM) mode.

Transmission electron microscopy (TEM)

Transmission electron micrographs (H-7650 Hitachi, Tokyo, Japan) were obtained to observe the morphology of the micelles. The samples were prepared by adding a drop of the polymer solution (0.1% w/v) on a copper grid (NS-C15 Cu150P; Stem, Tokyo, Japan). After drying at 10, 45, and 70 °C, the grid was negatively stained with 1% phosphotungstic acid (Sigma Aldrich, Steinheim, Germany) for 30 s, washed with a drop of distilled water, and air-dried.

Turbidimetry

The cloud points of the micelles were determined using UV-visible spectroscopy (UV-Vis; UV-1800, Shimadzu Corp., Kyoto, Japan). Each transmittance value was obtained at different temperatures during heating runs in steps of 2 °C at a wavelength of 550 nm, and the equilibration time at each temperature was 12 min.

Ultra-small-angle X-ray scattering

USAXS measurements were carried out at the BL08B2, SPring-8 (Harima, Japan) using an X-ray with a wavelength of λ = 0.10 nm and the distance from sample to detector of 16 000 mm.

The 2-dimensional USAXS data measured by Pilaus3-S-1M detector (172 μm square pixel size, DECTRIS) were converted into the one-dimensional intensity $I(q)$ as a function of the scattering vector q ($q = 4\pi \sin\theta/\lambda$, where 2θ is the scattering angle, beam width: 0.2 × 0.3 mm^2) by circular averaging. The covered range of q was 0.008–0.2 nm^{-1}.

PLLSA50-cho-PSPB was dissolved in double distilled water to 5% w/w and 10 μL of the solution was placed in a silicone mold (ϕ = 2 nm, thickness = 1 mm) and covered with Kapton film and loaded onto the sample chamber. Samples were measured in the temperature range of 5–50 °C at a heating speed of 5 °C min^{-1} by attaching a temperature-controlling plate (Linkam 10002L Cooling Stage, Linkam Scientific Instruments, UK). The exposure time was 30 s for each temperature.

The SAXS data can be analysed by following structure model.

$$I(q) = I_G(0)e^{-q^2R_g^2} + \frac{I_{DB}(0)}{(1+q^2\Xi_{DB}^2)^2} + \frac{I_{OZ}(0)}{1+q^2\xi_{OZ}^2} \quad (1)$$

The first term represents the Guinier raw, which can estimate the radius of gyration (R_g) of micelles and the intensity of Guinier raw at q = 0 ($I_G(0)$). The second and third terms account for the scattering originating from the inhomogeneous micelle assembly structure and the fluctuation intra-micelle, respectively. In the equation, Ξ_{DB} indicates the size of micelle assembly and ξ_{OZ} denotes the correlation length of thermal fluctuation.[64,65]

Cytotoxicity study

The cytotoxicity of the micelles was evaluated using the 3-(4,5-dimethylthiazol-2-yl)-2,5-Diphenyltetrazolium bromide (MTT) assay. L929 (American Type Culture Collection, Manassas, VA, USA) cells were cultured and treated with different concentrations of micelle solutions. First, 1 × 10^3 cells in 0.1 mL of culture medium were seeded on a 96-well plate and incubated for 72 h. Then, 0.1 mL of the culture medium with different concentrations of micelles was added to the 96-well plate. After

re-incubation for 24 h, 0.1 mL MTT (3-(4,5-dimethylthiazole-2-yl)-2,5-diphenyltetrazolium bromide) solution (300 μg mL^{-1}) was added to each well, and the cells were incubated for an additional 3 h. After removing the medium, (DMSO, 0.1 mL) was added to dissolve the purple formazan crystals formed by the living cells. Cells without micelle treatment were used as controls. The absorbance at 540 nm was measured using a microplate reader (versa max, Molecular Devices Co., CA, USA). Dulbecco's modified Eagle's medium (Sigma-Aldrich, St. Louis, MO, USA) supplemented with 10% heat-inactivated fetal bovine serum was used as the culture medium.

Results and discussion

Characteristics of copolymers

Dual-thermo-responsive polymers with cholesterol were synthesized by RAFT polymerization. As shown in Scheme 1, in the first step, carboxylated PLL was synthesized by adding different amounts of SA to ε-PLL.[37] The degree of substitution was determined by ^{1}H NMR spectroscopy (Fig. S1 and S2, ESI†) and was close to the feed ratio. (Table 1). In the next step, macro-CTA was synthesized by adding a controlled amount of RAFT agent to PLLSA. The incorporation of the RAFT agent was again evaluated using ^{1}H NMR spectroscopy, and the results showed that nearly 1 RAFT agent was introduced per chain of PLLSA (Fig. S3 and S4, ESI†), which is in accordance with the desired synthetic strategy (Table 1). Subsequently, a cholesterol-modified chain transfer agent was synthesized on the PLLSA backbone by reacting the macro-CTA with cholesterol chloroformate. A TNBS assay was used to determine the amount of cholesterol incorporated by estimating the free amino group before and after the reaction (Table 1). Fig. 1 shows the 2D ^{1}H–^{13}C heteronuclear single quantum coherence (HSQC) spectrum of Macro-CTA-cho. The addition of cholesterol increased the hydrophobicity of the polymer; thus, this NMR spectrum was obtained in DMSO-d_6. HSQC provides information on the correlation of two different nuclei separated by a single bond.[66] From this spectrum, the small peak that appears at δH = 5.2 ppm can be correlated with δC = 125 ppm (indicated by red circle in Fig. 1), which clearly shows that this peak represents the cyclic alkene group in the cholesterol moiety. This result indicates that a cholesterol modified-macro-chain transfer agent was successfully synthesized.

The macro-CTA was then used to polymerize SPB to yield copolymers of PLLSA-cho-PSPB. The number of repeating units of SPB in the feed was fixed at 200 for each polymer. To obtain micelles of different charges, PLLSA65 and PLLSA50, with two different degrees of substitution of SA in PLL, were synthesized to impart negative and neutral charges to micelles, respectively. The structure of the polymers was characterized by ^{1}H NMR and ^{13}C NMR spectroscopy, and the results are shown in the Supplementary Information (Fig. S5–S8, ESI†). The characteristics of the micelles are presented in Table 1. M1 indicates the

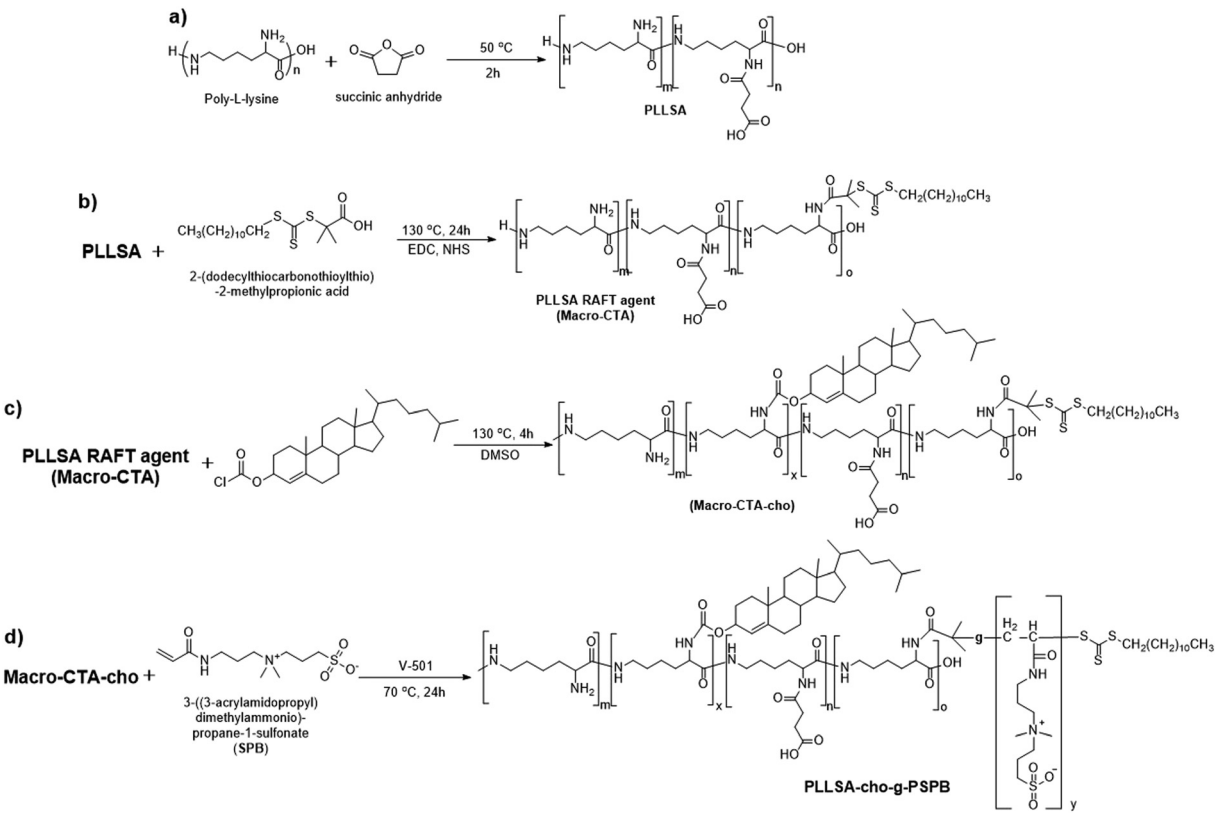

Scheme 1 Schematic of the synthesis of PLLSA-cho-PSPB.

Table 1 Characteristics of the PLLSA-cho-PSPB

Entry	Polymeric micelles	Degree of substitution of SA into PLL: In feed	Degree of substitution of SA into PLL: In polymer[a]	Number of RAFT agents substituted per chain[b]	Number of cho substituted per chain[c]	Number of repeating units: PLLSA	Number of repeating units: PSPB	M_w[b] $\times 10^{-3}$	Zeta potential
M1	PLLSA50-cho-PSPB	50%	47%	1.2	3.6	31.25	172.8	54.5	3.53 ± 0.142
M2	PLLSA65-cho-PSPB	65%	63%	0.9	1.9	31.25	132.8	43.8	−14.9 ± 0.872

[a] Determined using ^{1}H NMR. [b] Determined by subtracting the number of NH_2 groups in PLLSA from the RAFT agent substituted PLLSA. [c] Calculated using the TNBS assay.

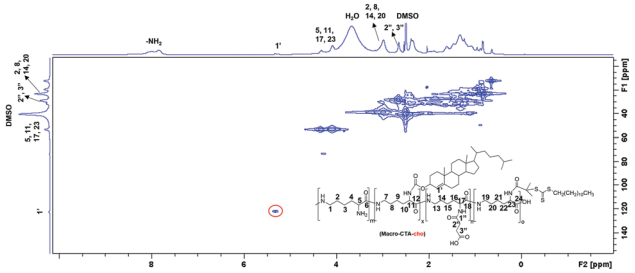

Fig. 1 ^{1}H–^{13}C HSQC spectra of Macro-CTA-cho in DMSO-d_6.

neutral charged micelle PLLSA50-cho-PSPB, and M2 indicates the negatively charged micelle PLLSA65-cho-PSPB.

Critical micelles concentration (CMC)

Micelle formation by the self-assembly of PLLSA-cho-PSPB was determined using pyrene as a fluorescent probe. Pyrene is highly hydrophobic and preferentially migrates into the core of the micelle in the aqueous solution.[67] The fluorescence of pyrene is quenched below the CMC of micelles. The fluorescence spectra of pyrene at different concentrations of M1 or M2 are shown in Fig. 2. An increase in the emission intensity indicates the transformation of a linear or random polymer structure into a micelle-like structure. Fig. 2(a) and (b) clearly show that the fluorescence intensity increases as the polymer concentration increases, indicating the formation of micelles.[68] The CMC was estimated from the intensity ratio of the peaks at 394 and 373 nm. The CMC of M1 and M2 was estimated to be approximately 6 μg mL^{-1} (Fig. 3(c) and (d)).

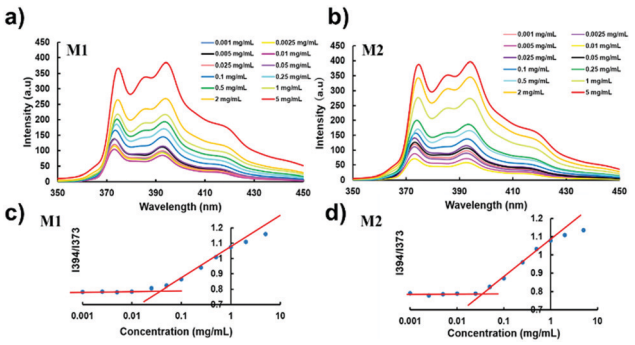

Fig. 2 Emission intensities of pyrene with polymers at various polymer concentrations of (a) M1 and (b) M2; plots of I_{394}/I_{373} in excitation spectra as a function polymer concentration: (c) M1 and (d) M2.

Thermo-responsive property

NMR spectroscopy. To evaluate the structural changes during the phase transition, temperature-dependent ^{1}H NMR spectroscopy was performed. The ^{1}H NMR spectra of M1 in D_2O obtained at different temperatures are shown in Fig. 3. It can be clearly seen that with an increase in temperature, the characteristic signals for the PLLSA block, with chemical shifts at 3.9 and 4.1 ppm, diminish in intensity and completely disappear at 75 °C. This indicates the reduced solubility of the PLLSA block with increasing temperature, which is a result of the shrinkage of the PLLSA block, indicating an LCST-type transition. In contrast, the intensity of the peak at 3.25 ppm, which is a characteristic peak of the PSPB block, became more prominent as the temperature increased. Papadakis and co-workers reported similar block copolymers of zwitterionic PSPB and PNIPAAM having UCST and LCST properties respectively. They demonstrated that these polymers forms "schizophrenic" micelles by a similar temperature dependent NMR method.[69] Our result indicates that the solubility of the PSPB part increases with increasing temperature, which may be due to the globule–coil transformation of the PSPB block. This result suggests that at high temperatures, the PLLSA and hydrophilic PSPB may act as the core and shell of the micelles, respectively, and *vice versa* at lower temperatures. Previous report supports

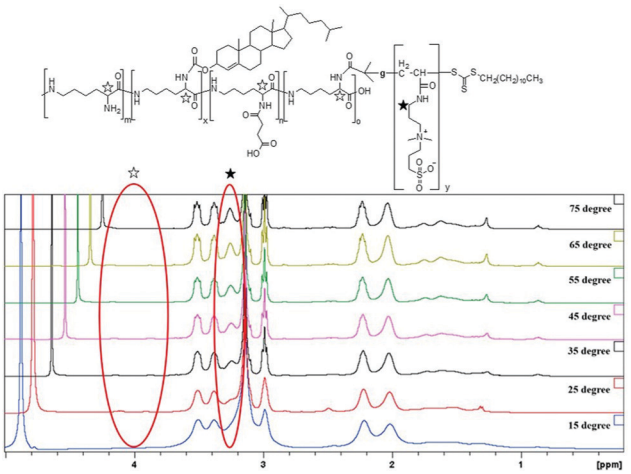

Fig. 3 Temperature dependent ^{1}H NMR spectra of M1 in D_2O. Temperature increases from 15 °C (bottom curve) to 75 °C (top curve) in steps of 10 °C.

the hydration changes of the block copolymer by temperature change through the shift of $\nu(SO_3^-)$ in IR spectra.[70]

UV-Vis spectroscopy. To determine the thermo-responsive property, the transmittance of 1% (w/w) polymeric micelle solutions was recorded at 550 nm at different temperatures. Fig. 4 clearly shows that the micelles display LCST- and UCST-type phase separation behavior. At low temperature (10 °C) and high temperature (70 °C), both M1 and M2 aqueous solutions appear turbid, which can also be seen by the low transmittance values at these temperatures. For M1 (Fig. 4(a)), from 10 to 20 °C, the transmittance of the micelle solution increased with increasing temperature. This behavior is because of the UCST property exhibited by the SPB segment in the micelle. With further increase in the temperature, the transmittance reaches a maximum value (at approximately 20 °C), indicating that here the polymer may exist in a linear form. When the temperature was increased further, the transmittance of the micelle solution started decreasing, which can be attributed to the exhibition of LCST property (from approximately 26 °C to 70 °C) by the PLLSA segment. The aqueous solution of M2 micelles also showed similar properties (Fig. 4(b)); the transmittance of the solution increased initially with increasing temperature (from 10 °C to 30 °C) and then decreased (from 30 °C to 70 °C). Interestingly, the increase in transmittance at low temperatures (for UCST) is sharp (higher slope), whereas at higher temperatures (for LCST), the curve for the decrease in transmittance is broader.[30] This is probably because the micelles consist of more UCST segments than LCST segments, that is, more repeating units of PSPB are present as compared to those of PLLSA.[61] Moreover, the maximum transmittance value of M1 was slightly lower than that of M2. This is because the amount of cholesterol introduced in M1 is higher than that in M2, which results in a lower solubility of micelles in an aqueous solution.

Particle size and zeta potential. The hydrodynamic diameter of micelles is an important factor that affects the drug loading, drug release, and bioavailability of the micelle. The temperature-responsive diameters of M1 and M2 were observed *via* dynamic light scattering (DLS) in water and are presented in Table 2 and Fig. 5. The micelle size was approximately 100 nm for M1 and M2 micelles, and this is reported to be suitable for cellular uptake and enhanced permeability and retention effect.[71,72]

The temperature responsiveness of both micelles also showed a similar behavior. At 10 °C, their micelle diameter was the largest, and their size decreased with increase in temperature and showed a small local maximum at approximately 45 and 35 °C for M1 and M2, respectively, and subsequently increased slightly with increasing temperature. Interestingly, the light scattering intensity (LSI) of M2 showed a continuous decrease. This indicates that the density of the micelles decreased. Since M2 has a small degree of substitution of cholesterol and excess anionic groups, loss of the molecules from the micelles might occur at higher temperatures because of weak packing and higher repulsion. This trend agrees well with the turbidimetry results.

Table 2 The diameter of micelles at different temperature estimated by DLS

Micelles	Temperature/°C	Diameter/nm
M1	10	103.9 ± 9.62
	45	81.4 ± 2.18
	70	80.7 ± 2.26
M2	10	129.1 ± 12.1
	45	101.3 ± 1.68
	70	109.1 ± 4.91

Morphology of micelles. The morphology of the micelles was observed by TEM and AFM. Fig. 6 shows TEM images of the 0.1% (w/w) M1 and M2 samples in water upon drying at different temperatures. As seen in Fig. 6, spherical micelles were obtained at all the temperatures. The size of micelles at different temperatures was almost similar to or smaller than those observed in the DLS results because of the drying process. The sizes of M1 and M2 micelles were larger at low temperatures and decreased with increasing temperature. As the temperature is lower than the UCST of PSPB, PSPB chains in the shell of micelles shrink and form a globular structure, leading to the aggregation of micelles. Then, the micelle size exhibited a constant decrease up to a temperature of approximately 35–45 °C. Above this temperature, simultaneous expansion of the PSPB chains and collapse of the PLLSA chain by LSCT balanced, and the micelle size exhibited complicated size changes. However, there was no significant difference in the sizes of the micelles at 45 °C and 75 °C. This may be owing to fewer repeating units of PLLSA. Moreover, the liquid–liquid phase separation may not lead to a significant change in size, although it brings the LCST to PLLSA.

Fig. S9 (ESI†) shows AFM images of M1 and M2. The concentration of the samples was 0.1% (w/w) in water. From the images, it is apparent that the size of each micelle was not uniform. This may be due to van der Waals interactions between the micelle structures. Also, we can observe that the

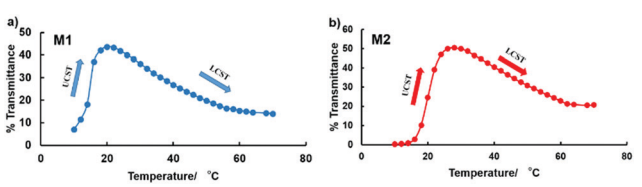

Fig. 4 Transmittance of polymeric micelle solutions of (a) M1 and (b) M2 relative to each other at 1% (w/w) in water.

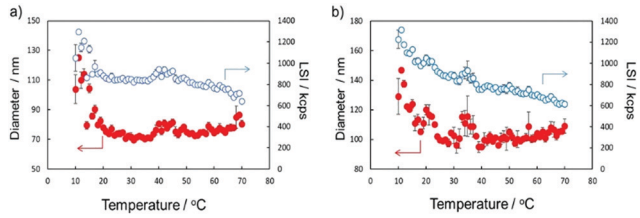

Fig. 5 Temperature dependent diameter and light scattering intensity (LSI) of M1 and M2.

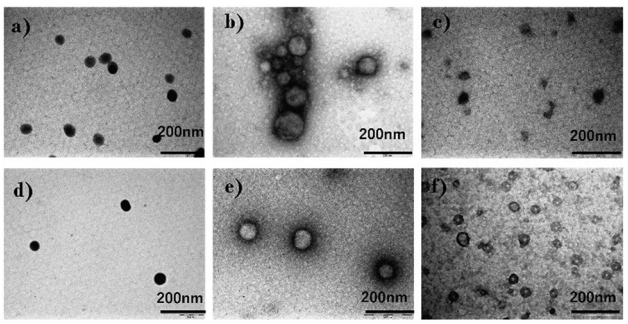

Fig. 6 TEM image of M1 (a–c) and (b) M2 (d–f) after drying the sample at different temperatures.

size of M1 is larger than that of M2. All TEM and AFM results correspond to the DLS results. The size of micelles obtained by DLS was larger than the sizes obtained by TEM and AFM owing to the extension of polymer chains in solution.

Ultra-small angle X-ray scattering results. Fig. 7 shows the USAXS curves obtained for M1 in water during heating. Upon increasing the temperature, the USAXS intensities at small q values decreased. In the case of PLLSA, which exhibited only the LCST-type property, a change in the intensity was observed in the high q region (Fig. S10(a), ESI†), whereas there was no change in the low q region. This indicates that the temperature-dependent changes at low q and high q represent USCT- and LCST-type phase separations, respectively.

The separation size (Ξ) at the low q region calculated using the Debye–Bueche function was approximately 350 nm (Fig. 8(a)). This can be explained by the large aggregation of micelles[73] which

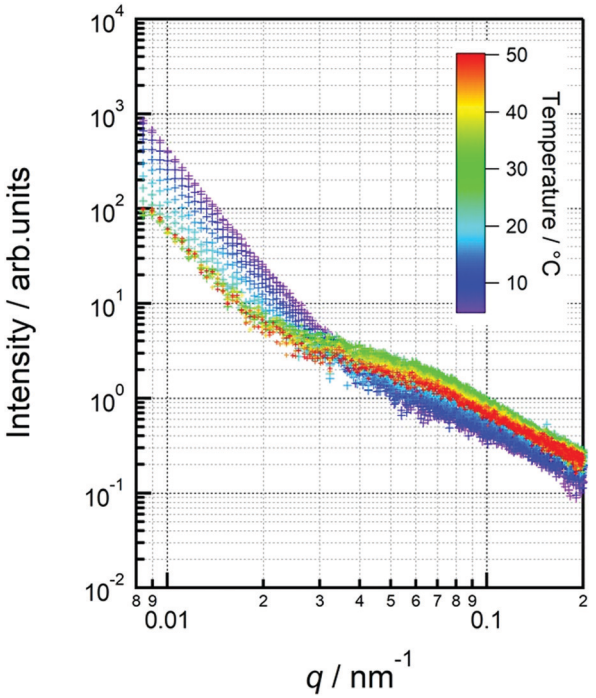

Fig. 7 USAXS curves of 5% w/w M1 at various temperatures in aqueous solution.

was diminished by the coil globule transition of the PSPB part at approximately 30 °C. In the high q region, the intensity of the q value increased with increasing temperature. This is due to the LCST-type phase separation of the PLL part. Then, we evaluated the Ornstein–Zernike approximation and calculated the correlation length (Fig. 8(a)). Although this value is smaller than Ξ, molecular-level fluctuations occurred in the LCST. In addition, the LCST was observed much earlier by USAXS analysis, as compared with UV-vis spectroscopy (Fig. 4); hence, USAXS analysis arguably detected the region of separation earlier. At the microscopic view, phase transition begins around 30 °C, and it might be correlated with the diminishing Ξ calculated using the Debye–Bueche function[74] in Fig. 8(a). O'Reilly and co-workers employed SAXS technique to demonstrate that temperature responsive transition from micelle to unimer takes place, and they revealed the critical temperature of micelle deformation detected by SAXS was lower than that detected by DLS.[75] Furthermore, the Guinier terms (R_g and $I_G(0)$) were invariant with respect to temperature change, which indicates that the average size and amount of the micelle are invariant. An example of fitted curves using Guimier, Denye–Bueche, and Ornstein–Zernike functions at 5 °C is shown in Fig. S11 (ESI†).

Interestingly, the USAXS results suggest that the UCST and LCST phenomena occurred at entirely different scales in terms of size. For UCST phenomenon in PSPB, a large change in particle size was observed at around Ξ_{DB} = 350 nm. This is likely due to the coil–globule transition in the PSPB. This is supported by the observation of spherical structures in TEM and AFM images. The actual difference in size might be owing to the high concentration of polymer in the SAXS analysis. The decrease in the Debye–Bueche intensity ($I_{DB}(0)$) during the SAXS analysis upon heating (due to UCST) indicates that the electron density contrast between particle and solution decreases because of the globule-to-coil transition. The disappearance of the intensity at 30 °C clearly indicates that some of the polymer chains could be dissolved in the solvent. This also agreed with the results of the light scattering intensity (LCI) decrease in DLS (Fig. 5(b)). In contrast, the LCST phenomenon in PLLSA was observed with a much smaller change in the size of the correlation length between the two phases with higher and lower densities. This might be due to the liquid–liquid

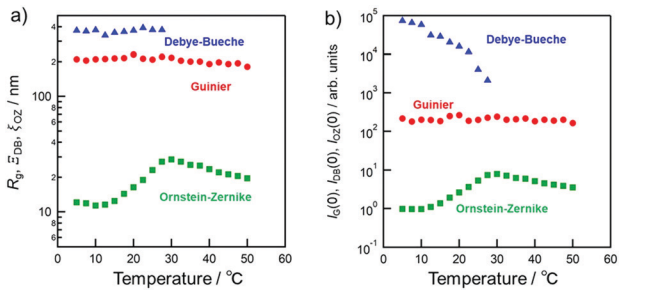

Fig. 8 Temperature responsiveness of (a) radius of gyration (R_g), Ξ_{DB}, and correlation length (ξ_{OZ}); (b) intensities IG(0), IDB(0), and IOZ(0) calculated using Guinier plot analysis at low q region and Debye–Bueche and Ornstein–Zernike plot analysis at high q region, respectively.

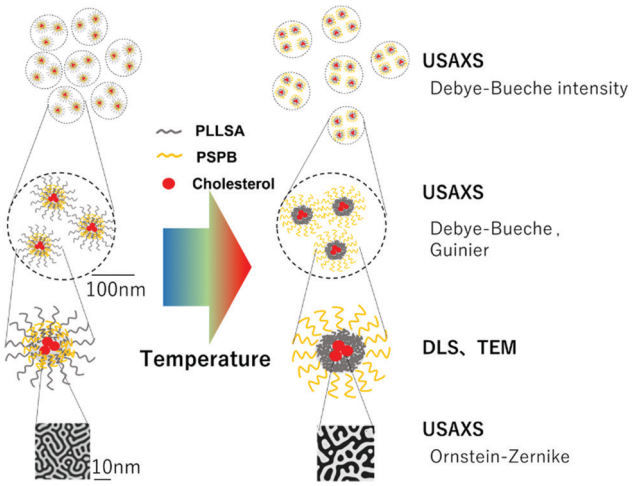

Fig. 9 Schematic illustration of thermoresponsive micelles structures change by various detection methods.

phase transition of PLLSA.[39] This was supported by the result that the value of this correlation length (ξ_{OZ}) was in the range of approximately 1–4 nm, which was similar to the values in the PLLSA molecules (Fig. S10(b), ESI†). From the results of UV-vis, TEM, AFM, DLS, and USAXS, it is possible that PLLSA-cho-PSPB formed micelles by self-assembly and the UCST type transition at lower temperature was caused by the PSPB chain coil–globule transition,[76] and the LCTS-type transition was caused by the PLLSA part through liquid–liquid phase transition with different size scales (Fig. 9).

Cytotoxicity

The cytotoxicity of polymeric micelles towards L929 cells was evaluated by the MTT assay, as shown in Fig. 10. The cell viability slightly decreased with the increase in the concentration of polymeric micelles, while the cell viability was still around 90% even at 1% concentration of polymeric micelles. This agrees well with the previously obtained low toxicity of PLLSA.[37,77] The negligible toxicity of the polymeric micelles shows that these micelles have great potential for use in delivering drugs or other cargoes into mammalian tissues.

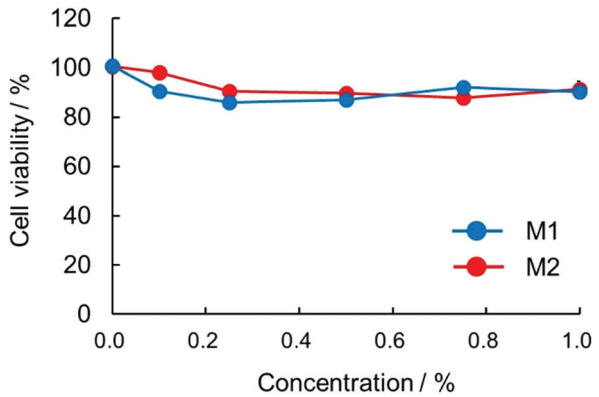

Fig. 10 Cytotoxicity of the micelles. L929 cells were treated with different concentrations of polymers: M1 (blue filled circles) and M2 (red filled circles).

Conclusions

Cholesterol-modified self-assembled micelles exhibiting UCST and LCST behavior in aqueous solutions were successfully synthesized. The spherical micelles were observed by TEM and AFM. Turbidimetric measurements showed that the structure of the micelles shrank and aggregated at low temperatures and high temperatures, respectively, and the chain of micelles extended and remained in the dissolved state at intermediate temperatures. Owing to the presence of PLLSA, the structure of micelles formed by self-assembly became complex. Both liquid–liquid phase separation and coil–globule transition were observed in our polymeric micelles. At low temperatures, the coil–globule transition of PSPB played an important role, whereas at high temperatures, liquid–liquid phase separation led to a decrease in transmittance. USAXS was employed to study the change in micelle structure with temperature. Interestingly, the phase transition temperature measured by USAXS was different from the temperature measured by UV-Vis spectroscopy. It was also found that the size scale of each phase transition of the UCST and LCST behaviors was completely different. This study provides detailed information on the structure of micelles containing the PLLSA segment. These micelles have potential applications in water-insoluble drug delivery systems and can be used for the protection of proteins owing to the presence of protein-stabilizing poly-SPB and PLLSA. Further studies are in progress to introduce degradability into such micelles, which will enable these micelles to successfully deliver therapeutic proteins inside the body.

Author contributions

Z. D.: writing – original draft, investigation, visualization; R. R.: conceptualization, methodology, project administration, supervision, writing – review & editing; S. Y.: investigation, visualization, funding acquisition; M. N.: investigation, visualization; K. M.: conceptualization, funding acquisition, methodology, project administration, resources, supervision, validation, writing – review & editing.

Conflicts of interest

There are no conflicts to declare.

Acknowledgements

This work was partially supported by Grants-in-Aid for Scientific Research (21H05535 (S. Y.), 21H05516 (K. M.)) from the Japan Society for the Promotion of Science (JSPS). The synchrotron radiation experiments were performed at the BL08B2 of SPring-8 with the approval of the Japan Synchrotron Radiation

Research Institute (JASRI) (Proposal No. 2018B3337 and 2019A3337).

References

1 C. Lu, L. Jiang, W. Xu, F. Yu, W. Xia, M. Pan, W. Zhou, X. Pan, C. Wu and D. Liu, *Colloids Surf., B*, 2019, **182**, 110384.
2 K. Jelonek, S. Li, X. Wu, J. Kasperczyk and A. Marcinkowski, *Int. J. Pharm.*, 2015, **485**, 357–364.
3 K. Rajagopal, A. Mahmud, D. A. Christian, J. D. Pajerowski, A. E. X. Brown, S. M. Loverde and D. E. Discher, *Macromolecules*, 2010, **43**, 9736–9746.
4 R. Savić, A. Eisenberg and D. Maysinger, *J. Drug Targeting*, 2006, **14**, 343–355.
5 H. Lee, F. Zeng, M. Dunne and C. Allen, *Biomacromolecules*, 2005, **6**, 3119–3128.
6 D. E. Owens and N. A. Peppas, *Int. J. Pharm.*, 2006, **307**, 93–102.
7 P. J. Photos, L. Bacakova, B. Discher, F. S. Bates and D. E. Discher, *J. Controlled Release*, 2003, **90**, 323–334.
8 T. Y. Kim, D. W. Kim, J. Y. Chung, S. G. Shin, S. C. Kim, D. S. Heo, N. K. Kim and Y. J. Bang, *Clin. Cancer Res.*, 2004, **10**, 3708–3716.
9 A. L. Z. Lee, S. Venkataraman, S. B. M. Sirat, S. Gao, J. L. Hedrick and Y. Y. Yang, *Biomaterials*, 2012, **33**, 1921–1928.
10 P. Laskar, S. Samanta, S. K. Ghosh and J. Dey, *J. Colloid Interface Sci.*, 2014, **430**, 305–314.
11 S. C. Kim, D. W. Kim, Y. H. Shim, J. S. Bang, H. S. Oh, S. W. Kim and M. H. Seo, *J. Controlled Release*, 2001, **72**, 191–202.
12 W. R. Sanhai, J. H. Sakamoto, R. Canady and M. Ferrari, *Nat. Nanotechnol.*, 2008, **3**, 242–244.
13 S. Mura, J. Nicolas and P. Couvreur, *Nat. Mater.*, 2013, **12**, 991.
14 C. J. F. Rijcken, O. Soga, W. E. Hennink and C. F. v. Nostrum, *J. Controlled Release*, 2007, **120**, 131–148.
15 D. Schmaljohann, *Adv. Drug Delivery Rev.*, 2006, **58**, 1655–1670.
16 P. Schattling, F. D. Jochum and P. Theato, *Polym. Chem.*, 2014, **5**, 25–36.
17 M. Joglekar and B. G. Trewyn, *Biotechnol. J.*, 2013, **8**, 931–945.
18 Y. Kotsuchibashi, *Polym. J.*, 2020, **52**, 681–689.
19 J. Zhao, V. E. Lee, R. Liu and R. D. Priestley, *Annu. Rev. Chem. Biomol. Eng.*, 2019, **10**, 361–382.
20 G. Ma, W. Lin, Z. Yuan, J. Wu, H. Qian, L. Xu and S. Chen, *J. Mater. Chem. B*, 2017, **5**, 935–943.
21 M. Patel, T. Kaneko and K. Matsumura, *J. Mater. Chem. B*, 2017, **5**, 3488–3497.
22 M. Patel, T. Nakaji-Hirabayashi and K. Matsumura, *J. Biomed. Mater. Res., Part A*, 2019, **107**, 1094–1106.
23 M. Karimi, P. Sahandi Zangabad, A. Ghasemi, M. Amiri, M. Bahrami, H. Malekzad, H. Ghahramanzadeh Asl, Z. Mahdieh, M. Bozorgomid, A. Ghasemi, M. Reza Rahmani Taji Boyuk and M. R. Hamblin, *ACS Appl. Mater. Interfaces*, 2016, **8**, 21107–21133.
24 S. Gammas, K. Suzuki, C. Sone, Y. Sakurai, K. Kataoka and T. Okano, *J. Controlled Release*, 1997, **48**, 157–164.
25 I. S. Kim, Y. Il Jeong, C. S. Cho and S. H. Kim, *Int. J. Pharm.*, 2000, **205**, 165–172.
26 A. Chilkoti, M. R. Dreher, D. E. Meyer and D. Raucher, *Adv. Drug Delivery Rev.*, 2002, **54**, 613–630.
27 C. De Las Heras Alarcón, S. Pennadam and C. Alexander, *Chem. Soc. Rev.*, 2005, **34**, 276–285.
28 S. Ganta, H. Devalapally, A. Shahiwala and M. Amiji, *J. Controlled Release*, 2008, **126**, 187–204.
29 A. Bordat, T. Boissenot, J. Nicolas and N. Tsapis, *Adv. Drug Delivery Rev.*, 2019, **138**, 167–192.
30 Y. Hu, V. Darcos, S. Monge and S. Li, *Int. J. Pharm.*, 2015, **491**, 152–161.
31 M. Heskins and J. E. Guillet, *J. Macromol. Sci., Chem.*, 1968, **2**, 1441–1455.
32 M. Sahn, T. Yildirim, M. Dirauf, C. Weber, P. Sungur, S. Hoeppener and U. S. Schubert, *Macromolecules*, 2016, **49**, 7257–7267.
33 R. Hoogenboom, *Angew. Chem., Int. Ed.*, 2009, **48**, 7978–7994.
34 S. Nayak, H. Lee, J. Chmielewski and L. A. Lyon, *J. Am. Chem. Soc.*, 2004, **126**, 10258–10259.
35 G. Pasparakis, A. Cockayne and C. Alexander, *J. Am. Chem. Soc.*, 2007, **129**, 11014–11015.
36 T. Wolf, T. Rheinberger, J. Simon and F. R. Wurm, *J. Am. Chem. Soc.*, 2017, **139**, 11064–11072.
37 K. Matsumura and S.-H. Hyon, *Biomaterials*, 2009, **30**, 4842–4849.
38 K. Matsumura, F. Hayashi, T. Nagashima, R. Rajan and S.-H. Hyon, *Commun. Mater.*, 2021, **2**, 15.
39 E. Das and K. Matsumura, *J. Polym. Sci., Part A: Polym. Chem.*, 2017, **55**, 876–884.
40 K. Zhang, M. Chen, K. J. Drummey, S. J. Talley, L. J. Anderson, R. B. Moore and T. E. Long, *Polym. Chem.*, 2016, **7**, 6671–6681.
41 F. Käfer, A. Lerch and S. Agarwal, *J. Polym. Sci., Part A: Polym. Chem.*, 2017, **55**, 274–279.
42 F. Käfer, F. Liu, U. Stahlschmidt, V. Jérôme, R. Freitag, M. Karg and S. Agarwal, *Langmuir*, 2015, **31**, 8940–8946.
43 P. Mary, D. D. Bendejacq, M. P. Labeau and P. Dupuis, *J. Phys. Chem. B*, 2007, **111**, 7767–7777.
44 N. Morimoto, Y. Oishi and M. Yamamoto, *Macromol. Chem. Phys.*, 2020, **221**, 1900429.
45 H. Kitano, T. Mori, Y. Takeuchi, S. Tada, M. Gemmei-Ide, Y. Yokoyama and M. Tanaka, *Macromol. Biosci.*, 2005, **5**, 314–321.
46 H. Kitano, T. Kondo, T. Kamada, S. Iwanaga, M. Nakamura and K. Ohno, *Colloids Surf., B*, 2011, **88**, 455–462.
47 R. Rajan, F. Hayashi, T. Nagashima and K. Matsumura, *Biomacromolecules*, 2016, **17**, 1882–1893.
48 R. Rajan, S. Ahmed, N. Sharma, N. Kumar, A. Debas and K. Matsumura, *Mater. Adv.*, 2021, **2**, 1139–1176.
49 K. Matsumura, R. Rajan, S. Ahmed and M. Jain, in *Biopolymers for Medical Applications*, CRC Press, Boca Raton, FL, 2016, pp. 165–182.

50 R. Rajan, Y. Suzuki and K. Matsumura, *Macromol. Biosci.*, 2018, **18**, 1800016.
51 R. Rajan and K. Matsumura, *Sci. Rep.*, 2017, **7**, 45777.
52 R. Rajan and K. Matsumura, *J. Mater. Chem. B*, 2015, **3**, 5683–5689.
53 Z. Dong, J. Mao, D. Wang, M. Yang, W. Wang, S. Bo and X. Ji, *Macromol. Chem. Phys.*, 2014, **215**, 111–120.
54 V. Butun, N. C. Billingham and S. P. Armes, *J. Am. Chem. Soc.*, 1998, **120**, 11818–11819.
55 P. L. Yeagle, *Biochimie*, 1991, **73**, 1303–1310.
56 Frederick R. Maxfield and Ira Tabas, *Nature*, 2005, **438**, 612–621.
57 P. L. Yeagle, *Biochim. Biophys. Acta, Biomembr.*, 1985, **822**, 267–287.
58 L. Hosta-Rigau, Y. Zhang, B. M. Teo, A. Postma and B. Städler, *Nanoscale*, 2013, **5**, 89–109.
59 Y. Wang, H. Wang, G. Liu, X. Liu, Q. Jin and J. Ji, *Macromol. Biosci.*, 2013, **13**, 1084–1091.
60 S. Zheng, Y. Xie, Y. Li, L. Li, N. Tian, W. Zhu, G. Yan, C. Wu and H. Hu, *Int. J. Nanomed.*, 2013, **9**, 55–66.
61 D. Zhao, R. Rajan and K. Matsumura, *ACS Appl. Mater. Interfaces*, 2019, **11**, 39459–39469.
62 A. Takahara, Y. Higaki, T. Hirai and R. Ishige, *Polymers*, 2020, **12**(7), 1624.
63 A. F. S. A. Habeeb, *Anal. Biochem.*, 1966, **14**, 328–336.
64 P. Debye, A. M. Bueche, P. Debye and A. M. Bueche, *J. Appl. Phys.*, 1949, **20**, 518–525.
65 E. Di Cola, C. Lefebvre, A. Deffieux, T. Narayanan and R. Borsali, *Soft Matter*, 2009, **5**, 1081–1090.
66 M. Elyashberg, *TrAC, Trends Anal. Chem.*, 2015, **69**, 88–97.
67 F. Zhou, H. Xu, Z. Song, L. Zhu, S. Feng and R. Feng, *New J. Chem.*, 2019, **43**, 444–453.
68 S. Ahmed, F. Hayashi, T. Nagashima and K. Matsumura, *Biomaterials*, 2014, **35**, 6508–6518.
69 N. S. Vishnevetskaya, V. Hildebrand, B. Niebuur, I. Grillo, S. K. Filippov, A. Laschewsky, P. Mu and C. M. Papadakis, *Macromolecules*, 2017, **50**, 3985–3999.
70 Y. Maeda, H. Mochiduki and I. Ikeda, *Macromol. Rapid Commun.*, 2004, **25**, 1330–1334.
71 F. R. Cheng, Y. J. Yang, Y. Liang, J. Q. Yan, J. Cao, T. Su, L. Jiang, B. He, X. L. Luo and Z. W. Gu, *RSC Adv.*, 2014, **4**, 62708–62716.
72 M. A. Subhan, S. S. K. Yalamarty, N. Filipczak, F. Parveen and V. P. Torchilin, *J. Pers. Med.*, 2021, **11**(6), 571.
73 S. C. Liao, C. S. Lai, D. Di Yeh, M. Habibur Rahman, C. S. Hsu, H. L. Chen and S. A. Chen, *React. Funct. Polym.*, 2009, **69**, 498–506.
74 M. Amann, J. S. Diget, J. Lyngsø, J. S. Pedersen, T. Narayanan and R. Lund, *Macromolecules*, 2019, **52**, 8227–8237.
75 K. E. B. Doncom, A. Pitto-Barry, H. Willcock, A. Lu, B. E. McKenzie, N. Kirby and R. K. O'Reilly, *Soft Matter*, 2015, **11**, 3666–3676.
76 Y. Higaki, M. Kobayashi and A. Takahara, *Langmuir*, 2020, **36**, 9015–9024.
77 K. Matsumura, S. Hatakeyama, T. Naka, H. Ueda, R. Rajan, D. Tanaka and S.-H. Hyon, *Biomacromolecules*, 2020, **21**, 3017–3025.